COBALT, NICKEL AND COPPER NAKED METAL CLUSTERS AND OLEFIN CHEMISORPTION MODELS *

GEOFFREY A. OZIN

Lash Miller Chemical Laboratories and Erindale College, University of Toronto, Toronto, Ontario (Canada)

(Received 19 September 1978)

CONTENTS

A. INTRODUCTION

The electronic, molecular, spectroscopic and chemical properties of small, naked metallic and multimetallic clusters of known size are of central concern to those interested in small-particle physics [1], nucleation phenomena [2], photographic processes [3], surface reaction intermediates [4], cluster theory [5], chemisorption models [4,6], alloy and bimetallic clusters [7,17], and heterogeneous catalytic phenomena [7]. However, the cluster-size regime below 10 Å (where the most dramatic excursions in physical—chemical properties with cluster size often occur) is a particularly difficult one to study, because of the limited availability of useful physical probes to establish very small cluster properties and the necessity to avoid the complication of further agglomeration. Metal atom cryo-deposition and bulk annealing techniques do, however, offer a means of controlling and investigating the embryonic steps of a series of nucleation events such as M → M_2 → M_3 → etc., as seen through the eyes of various techniques such as infrared, Raman, resonance-Raman, UV—visible absorption and emission, laser fluorescence, ESR, and Mössbauer spectroscopy, as well as via selective chemical reaction techniques [8].

Therefore, a new twist on an old method (matrix isolation) can provide a

---

* Originally presented as an invited lecture at the meeting on "Vibrations in Adsorbed Layers", Jülich, W. Germany, June, 1978.

rather unique opportunity for studying that age-old, yet still controversial, experimental/theoretical problem of metal-atom to metal-cluster to bulk-metal transformations. This type of research could lead naturally to an answer to the question of how many metal atoms and which geometric arrangements are required by a finite metal cluster for it to display properties representative of the bulk metal phase (e.g., ionization potential, cohesive energy, density of states, bandwidths, optical spectra, etc.).

More recently, cryophotochemical techniques have been developed which (i) allow a more controlled synthetic approach to mini metal clusters [9a], (ii) have the potential for tailor-making small bimetallic clusters (mini alloy clusters) [9b], (iii) permit the determination of relative extinction coefficients for naked metal clusters [9c], and (iv) allow naked cluster cryophotochemical experiments to be conducted in the range of just a few atoms or so [9d].

Selective interactions of these small metal clusters, M_n, with ligands, L, to yield $M_n L$ reactive intermediates, which are designed so as to bear a logical relationship to L chemisorbed on the corresponding bulk metal, M, have also been generated by these methods [4]. These finite cluster complexes can be considered to be ideal chemisorption models for use in testing "localized bonding" aspects of chemisorption (establishing boundary conditions) and for deciphering UPS data and vibrational HREELS data for chemisorbed L on bulk M.

The naked clusters and chemisorption models chosen for discussion in this paper are the recently-synthesized and cryochemically-immobilized few-atom systems M_n and $M_n(C_2H_4)_m$, where M can be Co [10,13], Ni [11,14], or Cu [9d,12,15] (n = 1, 2, 3 and m = 1, 2), and n, m can be systematically varied by way of metal-atom and ligand-concentration studies. For most of these small cluster systems, vibrational and UV—visible absorption spectral data have been collected. Whenever possible, the results will be discussed in the light of related Self Consistent Field $X\alpha$ scattered Wave molecular orbital (SCF-$X\alpha$-SW) and General Valence Bond Configuration Interaction (GVB—CI) molecular orbital calculations, and bulk-surface spectroscopic investigations.

B. NAKED METAL CLUSTERS

In view of the brevity of this review, detailed experimental discussions and theoretical interpretations have been omitted. Original papers are, however, referenced for clarification. To illustrate the cluster methodologies employed, representative systems have been judiciously selected and salient points have been emphasized.

The group VIII transition metals are renowned for their pervasive heterogeneous catalytic activity, particularly involving organic molecules [16]. Typically, olefin catalysis involves coordination of the unsaturated organic ligand at a single or multimetal surface site, followed by reactions often not observed for the free olefin; olefin isomerization, disproportionation and oligomerization provide familiar examples. Concomitant activation of small inorganic molecules (e.g., H_2, CO, O_2) along with the organic substrate leads in

these cases to hydrogenation, carbonylation/hydroformylation, and oxidation, respectively, of the organic ligand. Such catalysis remains the basis of more than 90% of commercial chemical processes.

Since the energy crisis has arrived, the petrochemical industries are intensively searching for alternative sources of energy and new ways to conserve existing energy and resources. One way of achieving such conservation is to improve the present understanding of existing heterogeneous catalyst systems, hoping thereby to gain greater product selectivity [17]. Ultimately, designed synthesis of new and better catalyst materials should evolve. A strategic move in this direction involves the investigation of metallic and bimetallic clusters in the few-atom regime, with the aim of extending the knowledge gleaned from microscopic systems to the macroscopic situation found in real, working particle catalysts. Chemical immobilization of these ultra-small metal aggregates could lead to materials with extremely potent catalytic properties. The metal aggregates Co_n, Ni_n and Cu_n will serve well to illustrate the type of information that may be extracted from studies of very small clusters, and the potential of the approach for elucidating the behaviour of their bulk particle analogs.

(i) Naked cobalt clusters

The cryodeposition metal atom technique for generating and identifying small clusters, as observed via their optical spectra, will be illustrated by reference to the cobalt system [10,13]. In brief, the optical spectrum of matrix-isolated cobalt atoms was first reported by Mann and Broida [18] in 1971. Slightly earlier, Kant and Strauss [19] (1966) observed the mass spectrum of Co atoms and Co_2 in equilibrium with liquid cobalt, and reported a bond dissociation energy for Co_2 of 39 ± 6 kcal mol^{-1}. Cooper et al. [20] in 1972 made use of the D_e data in an Extended Hückel Molecular Orbital (EHMO) study of Co_2 and concluded that partially-filled $3d$ orbitals can contribute to metal—metal bonding. Other than the studies mentioned above, little else was known about Co/Co_2, and no information existed for Co_3 or higher Co_n clusters.

Various approaches were adopted in a systematic search for dicobalt and higher-cobalt cluster optical absorptions. Evidence for cobalt atom aggregation at the "few-atom extreme" first came from a comparison of our optical data for Co/Ar = $1/10^4$ mixtures recorded at 4.2 K and at 10—12 K (see Fig. 1A, B). A differential of ~6—8 K in this cryogenic temperature regime was sufficient to cause the dramatic appearance of an entirely new set of optical absorptions in the regions 320—340 nm and 270—280 nm (Fig. 1A, B). Clearly, an overlap problem existed for some of the new lines (and caused confusion in our initial survey of the spectra of atomic cobalt) but it soon became clear from their temperature, cobalt concentration and matrix dependence that one was observing the embryonic stages of cobalt cluster formation. Using a Co/matrix ratio of ~$1/10^4$ and 10—12-K deposition condi-
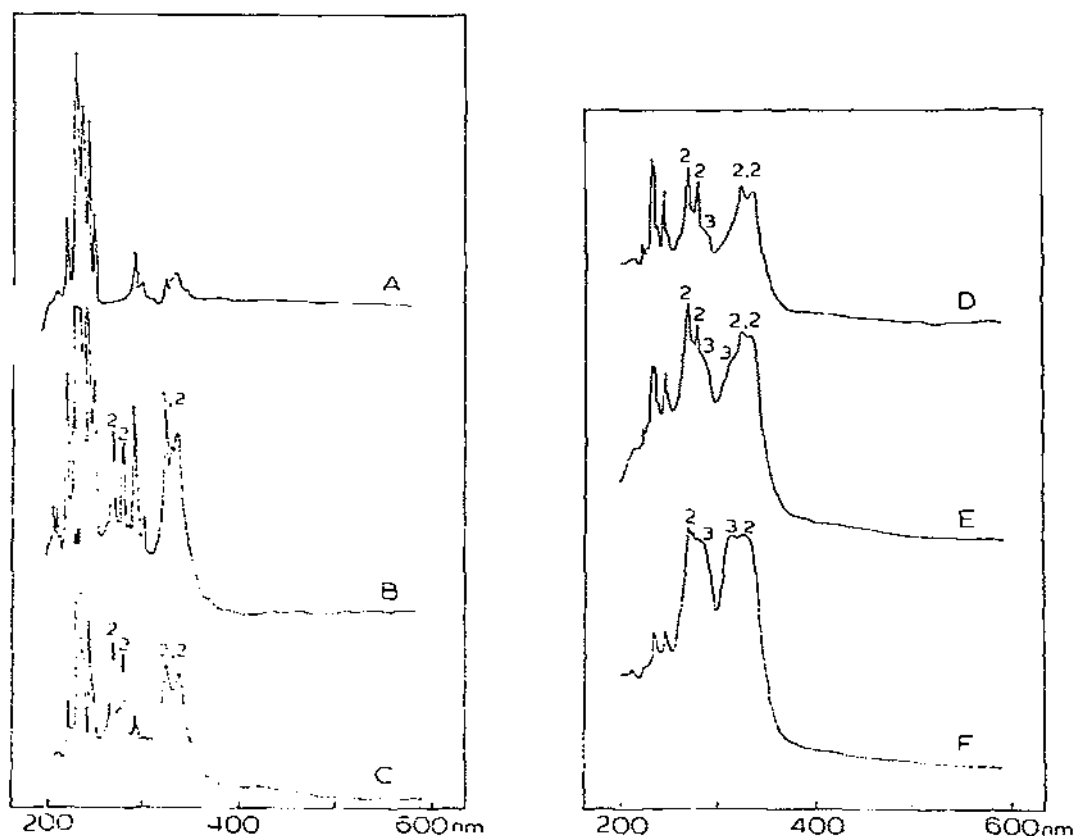
Fig. 1. The ultraviolet—visible spectra of Co/Ar ≃ 1/10⁴ mixtures deposited at (A) 4.2 K, (B) 10—12 K, (C) 20 K, (D) 25 K, (E) 30 K, and (F) 35 K, showing the gradual progression from isolated Co atoms to Co/Co_2 to $Co/Co_2/Co_3$ mixtures (ref. 13).

tions, one observes a monotonic decrease in the absorbance of the spectral features attributed to the first stage of the clustering process, as one passes from the more-mobile Ar matrix to the less-mobile, more-rigid krypton and xenon matrices (see Fig. 2A, B, C). This intensity ordering is entirely consistent with the more pronounced quenching efficiency of the more-polarizable, high-atomic-weight inert gas matrices and leads to the a priori assignment of dicobalt optical transitions listed in Table 1.

The effect of deposition temperature on the ability of cobalt atoms to form small cobalt clusters is most revealing in terms of both optical assignments and activation energy considerations. A series of runs with Co/Ar ratios ≃1/10⁴, deposited at 4.2, 10, 20, 25, 30, and 35 K is depicted in Fig. 1, part A—F, respectively. Between 4.2 and 10 K, the first stage of the cobalt-atom aggregation sequence of reactions makes itself apparent (Fig. 1A, B). On progressing to 20 K, a marked decrease in the cobalt atomic resonance lines rela-
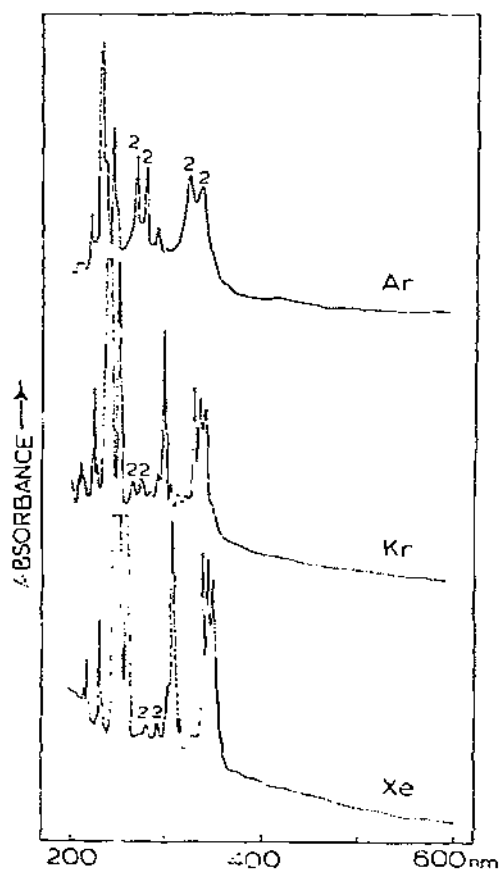
Fig. 2. The ultraviolet—visible spectra of Co/matrix $= 1/10^4$ mixtures deposited at 10—12 K in Ar, Kr and Xe (ref. 13).

tive to the new dicobalt spectral lines at 340, 320, 280 and 270 nm is already noticeable (Fig. 1C). On moving to 25—30-K deposition conditions (Fig. 1D, E), the effects observed at 20 K are considerably more pronounced but, significantly, the second stage of the cobalt clustering process is beginning to establish its presence, as witnessed by the growth of a new set of optical absorptions at approximately 287 and 316 nm with different growth/decay characteristics from those associated with Co and Co_2. The most dramatic realization of the presence of this third cobalt species is seen in the 35-K deposition (Fig. 1F), where the strongest cobalt atomic resonance lines have essentially decayed to zero; almost equal absorbances of dicobalt and the third cobalt species remain, and dominate the optical spectrum. Clearly the growth behaviour of this new cobalt species suggests an association with tricobalt. A large number of temperature and cobalt concentration [21] matrix experiments were performed and generally supported the contention of *three* dis-

122

TABLE 1

Observed and calculated (SCF-Xα-SW-MO) optical spectrum of dicobalt, Co_2

Observed (nm) [10,13]				Calculated (nm) [a,b,d]	Assignment [c,d]
Ar	Kr	Xe	CH_4		
340 [e]	321	—	345	353	$2\sigma_g^* \to 2\pi_u$
				355	$1\sigma_g^* \to 2\pi_u$
320	312	328	325	324	$1\sigma_u^+ \to 3\sigma_g^*$
280 [e]	284	290	283	305	$1\sigma_g^* \to 2\sigma_u^+$
270	274	279	274	247	$1\sigma_g^* \to 2\pi_u$
				252	$1\pi_u \to 3\sigma_g^*$

[a] $2\sigma_g^* \to 2\sigma_u^+$ calculated at 484 nm, which is in the region of extremely weak absorptions, possibly associated with Co_2. [b] Cobalt—cobalt bond length = 2.32 Å. [c] Ground state configuration $(1\sigma_g)^2(1\pi_u)^4(1\delta_g)^4(2\sigma_g)^2(1\delta_u)^4(1\pi_g)^2$. [d] Preliminary values obtained from ground-state transition energies; detailed spin-unrestricted, transition-state calculation will be reported later [10]. [e] Narrow band, continuous photoexcitation in these bands causes photobleaching of all of the dicobalt absorptions.

tinguishable, small cobalt cluster species, ascribed to Co, Co_2, and Co_3.

To complement these data we have calculated the electronic energy levels for Co_2, and for linear and non-linear Co_3 using the SCF-Xα-SW molecular orbital procedure [10]. Preliminary spin-unrestricted calculations of the optical spectrum for dicobalt were found to agree quite well with the observed spectra, as seen by reference to Table 1. Partial wave analyses showed that the s-band overlaps the d-band in Co_2 (as in Co metal itself), leading to significant 4s character in the formally 3d-derived $1\sigma_g^*$ orbital and to 3d character in the formally 4s-derived $2\sigma_g^*$ orbital, suggesting the qualitative conclusion that the bond in Co_2 has a significant d-contribution. From data of this type one can begin to appreciate the early development of the dsp orbital structure of larger cobalt clusters and the genesis of the band picture and optical properties of cobalt metal itself. Of significance here is the already close approach of the absorption spectrum of Co_3 (316, 287 nm) to the proposed optical transitions reported for massive Co particles and bulk Co films, which show maxima around 250—325 nm [22].

(ii) Naked copper clusters

Rather than exclusively attacking the nucleation problem by the more common metal-atom (single- or two-component) cryodeposition and bulk matrix annealing techniques, the limitations and strengths of which have both been adequately documented [4], we have searched for a more controlled and, hopefully, more versatile photochemical approach for the generation and study of very small naked metal clusters. A promising method which we have

recently discovered and termed "cryophotoclustering" is presently showing great potential for achieving cluster size distributions not hitherto accessible by conventional metal atom techniques [9]. The trick essentially involves narrow-band, continuous irradiation into the atomic resonance absorptions of matrix-entrapped metal atoms. One envisages atomic excitation, some non-radiative electronic-to-lattice phonon energy transfer, local warming and softening of the surrounding matrix cage, atom photomobilization (bulk diffusion) and subsequent photoaggregation to diatomic and higher metal clusters. [44]. Cluster sizes are envisaged to be dependent on metal concentration, the matrix material, matrix temperature, excitation wavelength and light intensity. In practice, one observes a highly controlled and selective photoclustering phenomenon which appears to be amenable to analysis by conventional solid-state diffusion kinetic theory [9c,23]. Cluster size determination appears to be possible using these methods [9c,23]. An additional bonus of the photoaggregation method is its ready extension to bimetallic cluster systems, in which photoselective clustering has already been demonstrated for the two combinations Cr/Mo/Ar [9b] and Cr/Ag/Ar [24], as well as others [43].

In the context of this discussion, the copper system [12] will serve to illustrate the cryophotoaggregation phenomenon [9d]. Its extension to the selective cryophotochemistry of Cu_2 will also be discussed. SCF-$X\alpha$-SW calculations will be employed to help rationalize the optical spectrum and matrix photochemistry of Cu_2 [9d].

A typical series of optical spectral traces which illustrate the cryophotochemistry of Cu atoms is shown in Fig. 3. For instance, Fig. 3A shows the absorptions of isolated Cu atoms in the presence of small amounts of Cu_2 and traces of Cu_3 molecules, obtained after a deposition with Cu/Ar $\simeq 1/10^4$ at 12 K [9d,12]. Under these concentration conditions the outcome of 300-nm narrow-band photoexcitation of atomic copper is photoaggregation up to the Cu_3 stage as depicted in Fig. 3B, C. The growth—decay behaviour of the various cluster absorptions allows one to unequivocally pinpoint ultraviolet—visible electronic transitions associated with Cu_2 and Cu_3 (Fig. 3B, C).

With the distribution of $Cu_{1,2,3}$ clusters shown in Fig. 3C, one can turn to 370-nm narrow-band excitation, and thereby test the feasibility of selective photodissociation and nucleation events associated with dicopper itself. For example, the outcome of 30 minutes continuous irradiation of Cu_2 is illustrated in Fig. 3B. The growth (~10%) of the Cu atomic resonance lines is immediately apparent from these optical spectra. The concomitant *growth* of Cu_3 and decay of Cu_2 under these matrix concentration conditions is also noticeable.

The spectral effects described above point to a clear-cut case of a Cu_2 photodissociation process, localized within the confines of the surrounding matrix cage, as one of the non-radiative energy channels preceding Cu_2 photoexcitation. The energy available at 370 nm (3.35 eV) considerably exceeds the gas-phase (mass spectral) bond dissociation energy of Cu_2 (1.95 ± 0.09 eV) [25]. Presumably part or all of this excess energy appears in kinetic form as a trans-
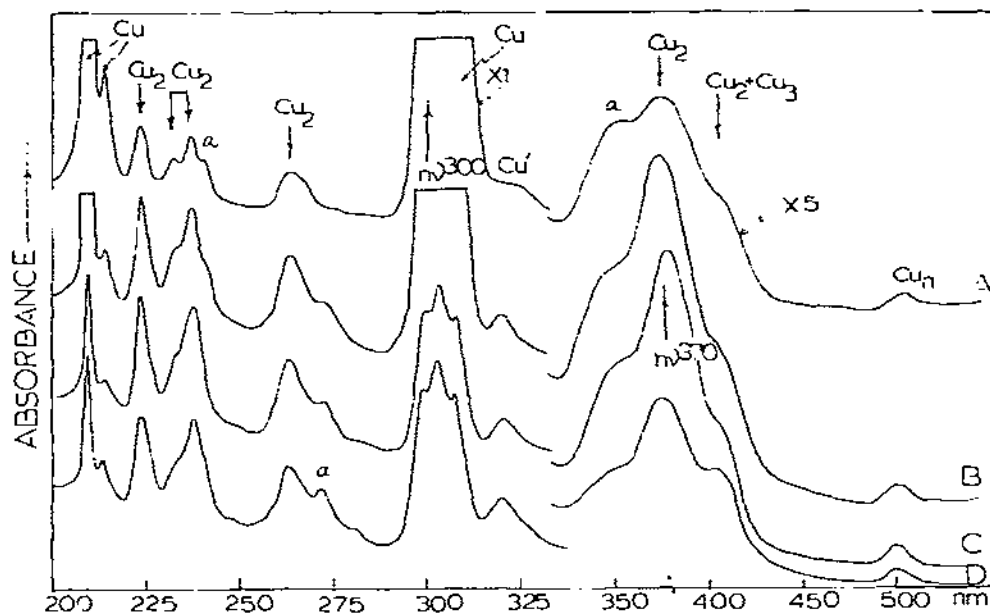
Fig. 3. The optical spectrum of a Cu/Ar ≃ 1/10⁴ mixture deposited at 12 K: (A) showing
isolated Cu atoms and Cu_2 molecules with a trace of Cu_3; (B) and (C) after 30 and 30
minutes, respectively, of 300-nm narrow-band continuous photoexcitation of the Cu
$^2S_{1/2} \rightarrow {}^2P_{3/2,1/2}$ resonance line, showing photoaggregation to the $Cu_{2,3}$ stage; (D) after
30 minutes of 370-nm narrow-band continuous photoexcitation of the lowest energy
absorption of Cu_2, showing photodissociation to Cu atoms and further aggregation to Cu_3.
SCF-Xα-SW optical assignments for Cu_2 (and Ag_2) are included in Table 3 (ref. 9d). The
features marked "a" are thought to arise from secondary trapping sites of Cu_2.

lationally-mobile Cu atom ejected from its matrix cage, culminating with Cu
atom isolation and formation of higher clusters such as Cu_3. Concurrent pro-
cesses that must also be considered during Cu_2 visible photolysis will be
described in another paper.

Cu_2 is particularly suited for cryophotochemistry experiments for two
reasons. First, its spectra have been rather thoroughly studied, both in the gas
phase at high temperatures [26] and in inert-gas matrices at low temperatures
[9d,12]. Vibration—rotation analyses of the gas-phase spectra have produced
precise values for the $0 \rightarrow 0$ transition energies, metal—metal stretching fre-
quencies, and, for Cu_2, the internuclear distance (2.2195 Å). Dissociation ener-
gies have been obtained from mass spectra [25]. The assignments proposed
for the experimentally-observed electronic transitions and from simple MO
calculations of the extended-Hückel or CNDO type [20,27] serve as a guide
to selection of transitions for the photochemical studies.

Second, the inherently simple electronic structure expected for Cu_2 further
aids the design and interpretation of the photochemical experiments. The
metal—metal bonds should largely involve simple pairing of the s electrons on
the two $d^{10}s^1$ metal atoms. One of the lowest-energy absorptions should there-

fore involve excitation from the bonding $s\sigma_g$ to the antibonding $s\sigma_u$ orbital. Although in the gas phase simple photodissociation is the likely outcome of such excitation, a much larger number of photophysical and photochemical events can be envisaged in the matrix. Our interpretation of the results of irradiation at 370 nm suggests that the $s\sigma_g \rightarrow s\sigma_u$ transition of Cu_2 does lie in this region. Let us now turn to the salient features of our SCF-$X\alpha$-SW calculations for Cu_2, which provide an interpretation of the electronic spectrum and help explain the observed photochemistry [9d].

The efficient use of the real $X\alpha$-SW density to calculate the total energy remains an unsolved problem, although notable progress has been made [28]. The one case where the present approximate total energy should yield a reasonable potential curve is where the bonding is mainly due to interaction of s orbitals, that is, spherically-symmetric densities around each atom. The comparison of our calculated potential curve for Cu_2 (and Ag_2) with experiment, shown in Table 2, confirms that this hypothesis is correct. The metal—metal stretching frequency, reflecting the shape of the potential curve, is calculated to within 6 cm^{-1} of the experimental value. The bond distance for Cu_2 is within 0.05 Å of the experimental value. The dissociation energy for Cu_2 is slightly high; this quantity is known to be especially difficult to calculate from first principles, using even the best one-electron total energy methods. For Cu_2 we used the experimental distance of 2.22 Å to discuss the equilibrium one-electron properties of the molecule. The orbital picture that emerges from these calculations is shown in Fig. 4 (the scheme for Ag_2 is included for comparison). The bound valence orbitals include, in order of increasing energy, the six completely-filled σ, π and δ bonding and antibonding d-band levels, the s-band with an occupied σ-bonding and an empty σ-antibonding level, and empty π and σ bonding levels from the p-band.

The s-band overlaps the upper part of the d-band in Cu_2. The d-like $1\sigma_u$ and $1\pi_g$ levels are thus the highest-occupied levels in Cu_2. As can be seen from Fig. 4, this is a consequence of the small separation of the d and s atomic

TABLE 2

Equilibrium bond distances, metal—metal stretching frequencies, and dissociation energies for Cu_2 and Ag_2 [a]

	r_e (Å)	ν(M—M) (cm^{-1})	D_e(kcal/mole^{-1})
Cu_2			
Calculated [e]	2.17	272 ± 5	66 ± 1
Experimental	2.22 [b]	266 [c]	45 ± 2 [d]
Ag_2			
Calculated [e]	2.84	187 ± 2	36 ± 3
Experimental	?	192 [c]	38 ± 2 [d]

[a] Where estimated errors are not indicated, they are smaller than the last figure tabulated.
[b] Ref. 29. [c] Ref. 26. [d] Ref. 25. [e] Ref. 9d.

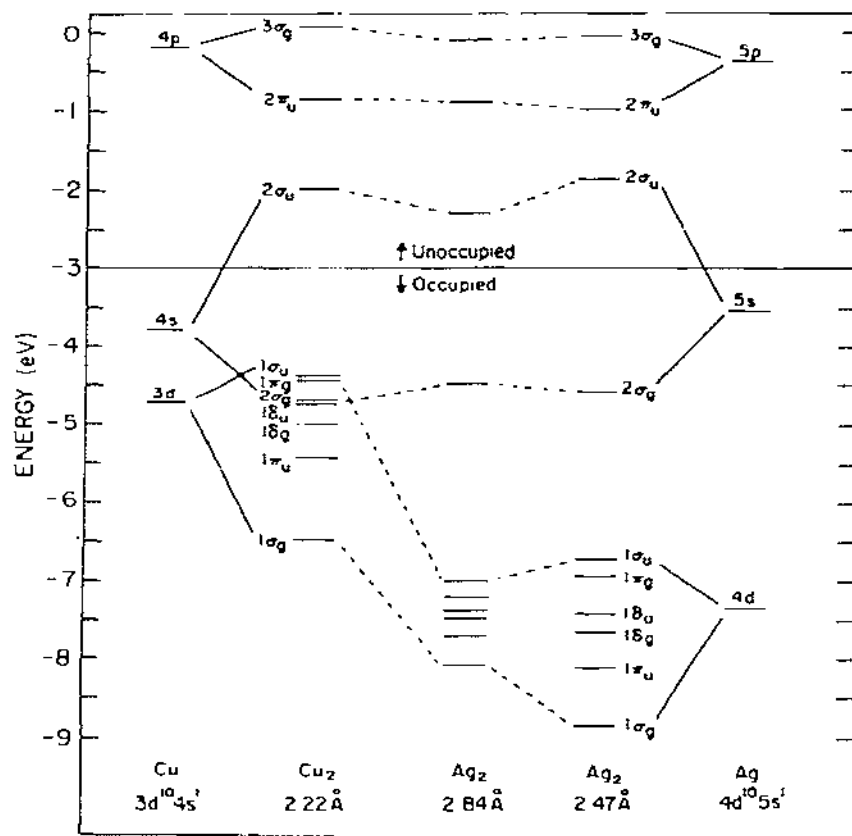Fig. 4. Ground state SCF-Xα-SW valence energy levels for Cu/Cu₂/Ag/Ag₂. The bands of molecular levels most closely correlating with atomic d, s and p levels are indicated (ref. 9d).

levels in Cu. It leads in Cu_2 to significant mixing of $4s$ character into the formally $3d$-derived $1\sigma_g$ orbital, and of $3d$ character into the formally $4s$-derived $2\sigma_g$ orbital. Figure 5 provides a pictorial representation of the $2\sigma_g$ and $2\sigma_u$ wavefunctions for Cu_2 and Ag_2.

The symmetry of the occupied-orbital manifolds alone dictates that there is a net single bond of σ type in both molecules. The relative d-s-p character of this net bonding turns out to be 73% s, 17% d, and 10% p for Cu_2 [9d], and 91% s, 1% d, and 8% p for Ag_2 [9d]. A reasonable qualitative conclusion is that the bond in Cu_2 has a small but significant d contribution whereas that of Ag_2 is essentially pure s.

Table 3 shows the assignment of the electronic transitions of Cu_2 observed in the gas phase at 2000—2300 K and in solid argon at 12 K. The calculated positions specifically represent the singlet (spin-allowed) components and include orbital relaxation between ground and excited states.

For Cu_2 there are broad, visible absorptions and a number of sharper UV

TABLE 3

Calculated and experimental electronic spectra of Cu_2 and Ag_2 ($\times 10^3$ cm^{-1})

Transition	Calculated [a]	Experimental			
		Gas [b]	Ar[9d,12]	Kr[9d]	Xe[9d]
Cu₂					
$1\pi_g \rightarrow 2\sigma_u$	24.1(0.02)	20.4	25.0	25.0	25.0
$2\sigma_g \rightarrow 2\sigma_u$	26.5(0.32)	21.7	27.0	27.0	27.8
$1\pi_g \rightarrow 2\pi_u$	35.2(0.15)		38.2	37.0	35.1
$2\sigma_g \rightarrow 2\pi_u$	37.2(1.02)		41.7/42.4	41.5/42.0	40.5/41.0
$1\delta_g \rightarrow 2\pi_u$	39.5(0.13)		43.1	42.7	41.7
$1\sigma_g \rightarrow 2\sigma_u$	39.8(0.36)		44.8	44.0	43.1
$1\sigma_u \rightarrow 3\sigma_g$	43.7(0.03)				
Ag₂		Gas	Ar[9a,d]	Kr[9a,d]	Xe[9a,d]
$2\sigma_g \rightarrow 2\sigma_u$	22.0(0.64); 25.7(0.63)	23.0	24.3/25.8	25.6	25.6
$2\sigma_g \rightarrow 2\pi_u$	33.2(1.33); 33.6(1.37)	37.6	37.8/38.3	35.5/37.0	34.5/35.3
$1\pi_g \rightarrow 2\sigma_u$	43.5(0.03); 45.6(0.04)	40.2	44.1	45.0	46.1

[a] All spin- and dipole-allowed transitions below 48 and 51 $\times 10^3$ cm^{-1} for Cu_2 and Ag_2, respectively [9d]. For Ag_2, the first value is for 2.84 and the second for 2.47 Å. Oscillator strengths are given in parentheses. [b] $0 \rightarrow 0$ transitions, from ref. 26 for Cu_2 and from ref. 42 for Ag_2. The weak B ← X and D ← X bands of Ag_2 at 35.8 and 39.0 $\times$ cm^{-1}, believed to be due to forbidden transitions, are omitted.

absorptions in the matrix spectrum (see Fig. 3) [9d,12]. The visible absorption appears to have two maxima near 25 and 27 $\times 10^3$ cm^{-1}, corresponding to the matrix-shifted A ← X and B − X systems observed in the gas phase (see Table 3). The UV region displays maxima near 38, 42 and 44 $\times 10^3$ cm^{-1}, with distinct shoulders at 41 and 43 $\times 10^3$ cm^{-1} [9d,12]; there are no corresponding data for the gas phase. The calculations again predict transitions in close correspondence with experimental observations. The A ← X and B ← X systems are assigned to $d\pi^* \rightarrow s\sigma^*$ and $s\sigma \rightarrow s\sigma^*$ transitions, respectively. This agrees with the conclusion, from the vibration—rotation analysis of the gas-phase spectrum, that A ← X is of $^1\Sigma_g^+ \rightarrow {}^1\pi_u$ and B ← X of $^1\Sigma_g^+ \rightarrow {}^1\Sigma_u^+$ type [29]. Moreover, the observation [30] that gas-phase B ← X is stronger than A ← X agrees with the predicted symmetries ($\sigma \rightarrow \sigma^*$ compared to $\pi^* \rightarrow \sigma^*$). It is more difficult to assign the five observed high energy maxima to individual transitions, even though five are predicted in this region. Based on calculated positions and intensity considerations we assign the UV bands of Cu_2 (and Ag_2) according to the scheme shown in Table 3.

The critical feature of these assignments relating to our photochemical experiments is that the wavelengths used for photoexcitation are essentially those of the $2\sigma_g \rightarrow 2\sigma_u$ transition, that is, the $s\sigma \rightarrow s\sigma^*$ excitation which should be capable of disrupting the metal—metal bond. Thus, the observed formation of Cu atoms as one of the products of 370-nm Cu_2 photoexcita-

tion is consistent with predictions from the SCF-$X\alpha$-SW calculations [9d].

With atomic and diatomic photoselectivity at hand, one can begin to consider the exciting possibility of extending the method to the photochemistry of higher naked cluster systems by simply performing narrow-band irradiations into carefully-chosen molecular absorptions of M_n as a function of n. If generally applicable, the method offers the unique opportunity of observing "naked cluster transformations" and generating "naked cluster distributions" which cannot be approached by any other known physical or chemi-

129
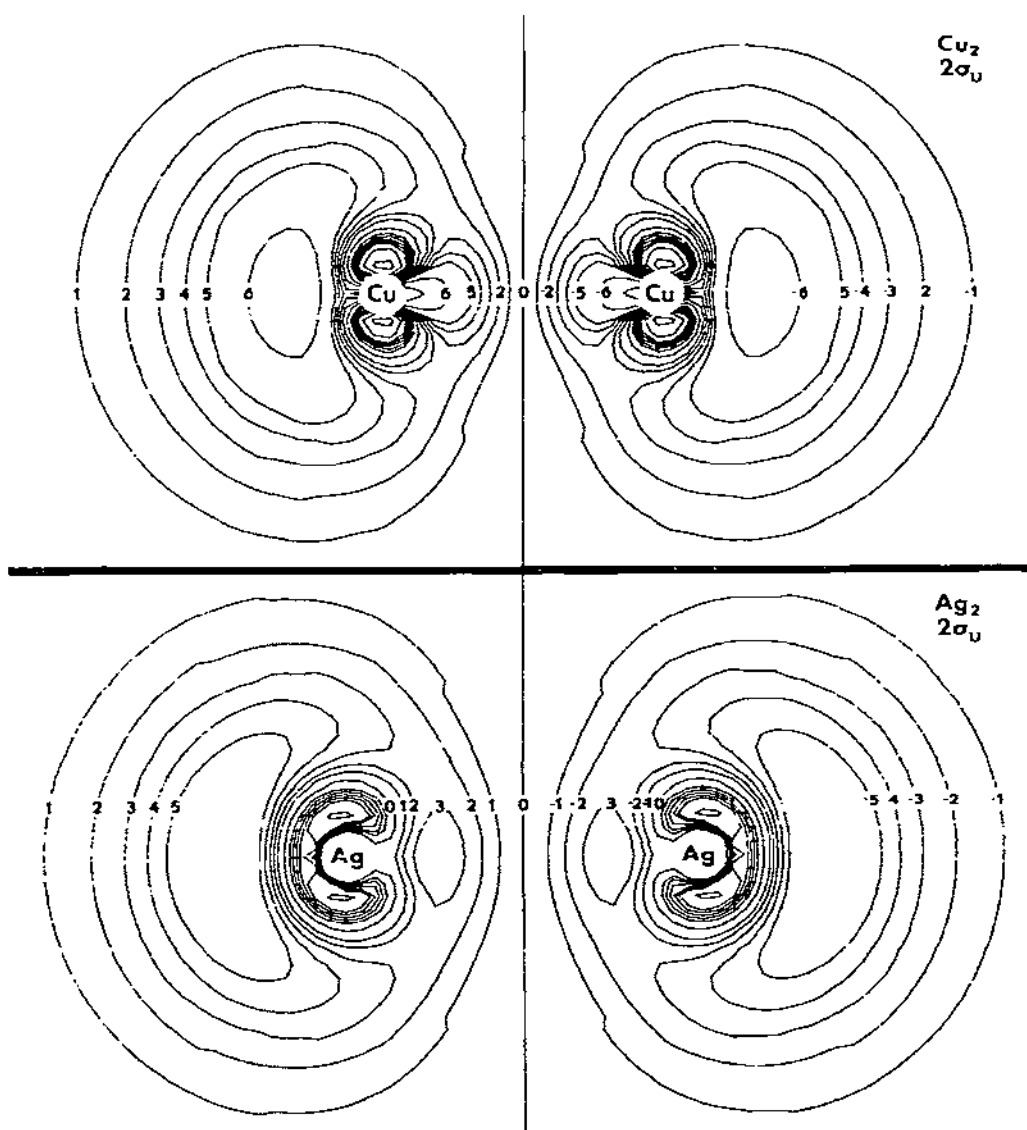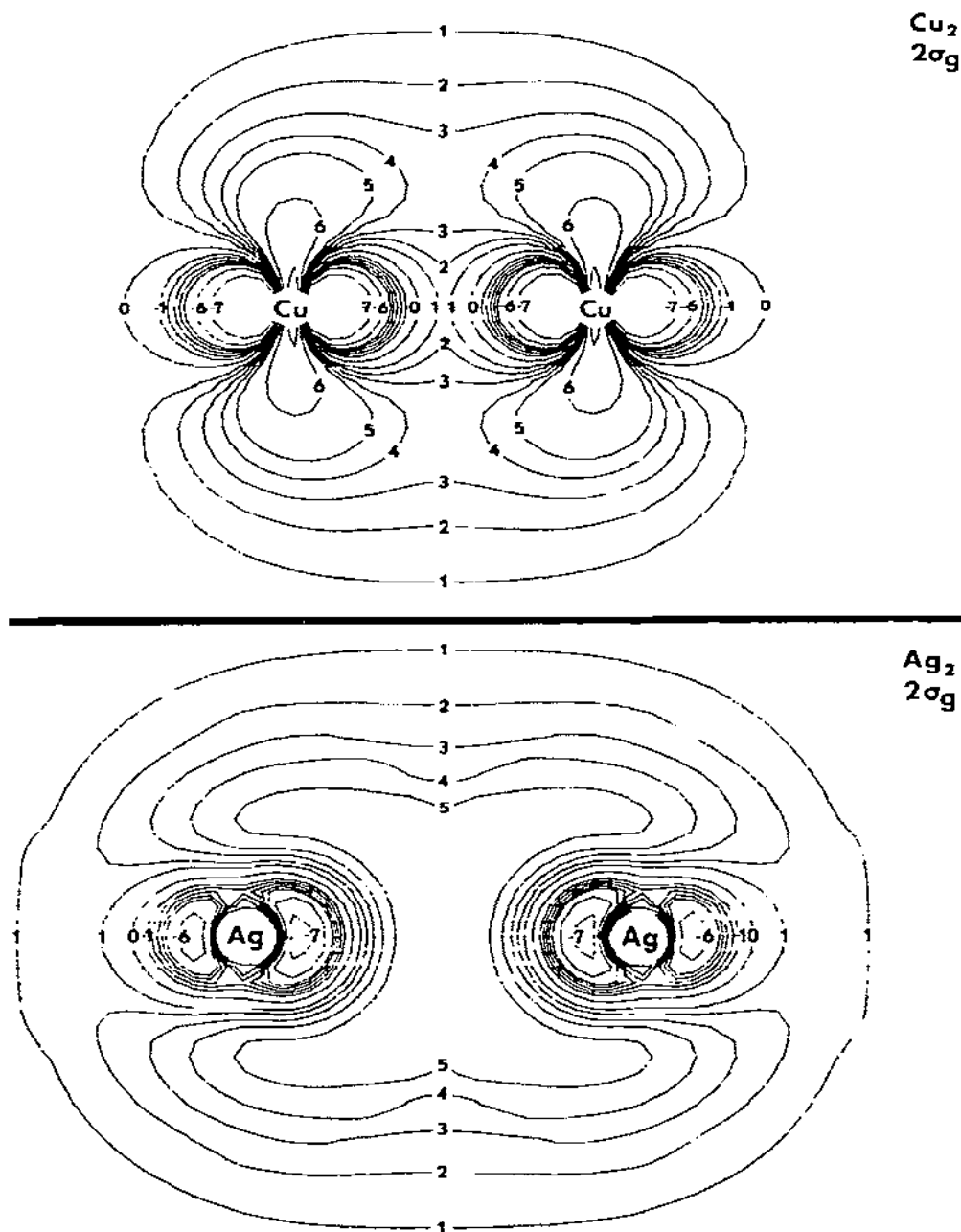
Fig. 5. Contour maps of the wavefunction for the mainly s-bonding and mainly s-antibonding orbitals of Cu₂ and Ag₂ at 2.22 and 2.84 Å. Note the significant amount of d-character in the $2\sigma_g$ orbital of Cu₂ (ref. 9d).

cal technique or probe. Moreover, an insight into cluster excited states by way of predicted cluster transformations may be an additional bonus of the method (photoisomerization, photodissociation, photoaggregation, photo-ionization, etc.). The significance of these studies in the fields of organometallic cluster photochemistry, photocatalysis, and photography, to name but a few, could prove to be considerable. Photoselective sintering techniques may even emerge from such investigations which, if realized, could have a considerable impact on the future development of a new generation of supported catalyst systems.

C. OLEFIN CHEMISORPTION MODELS

Often, the theorist who wishes to gain an insight into the geometrical, electronic, bonding and chemical properties of surface reaction intermediates, simplifies the complex surface problem by representing the active site in terms of a finite chemisorption model of the form M_nL, where M_n depicts a cluster of metal atoms (whose size and shape can by systematically varied) interacting with a chemical entity L (which may be atomic, free radical or molecular) [5,6,31]. Of central concern to the validity of this "localized bonding" description of adsorbate—adsorbent interactions is the convergence behavior of the calculated molecular and electronic properties of M_nL with respect to the bulk chemisorption situation per se. To assess the usefulness of finite cluster representations of bulk chemisorption phenomena, one would ideally like to synthesize and spectroscopically (and if possible chemically) evaluate a reasonably large cross-section of "super-coordinatively unsaturated" M_nL chemisorption models as a function of metal cluster size n [4].

Until very recently, only very limited vibrational and electronic spectral data existed which were common to both the M_nL and $M(L_{ads})$ systems. However, with the emergence of High-Resolution Electron Energy Loss Spectroscopy (HREELS) as a powerful new probe for studying surface atomic and molecular vibrational [32] and electronic excitations [33], it now becomes feasible to bridge the "fuzzy interface" between finite M_nL and bulk $M(L_{ads})$ systems. In principle, meaningful assessments can now be made of the extent of localization of metal—ligand interactions in the vicinity of a chemisorption site.

Homogeneous and heterogeneous catalytic reactions involving transition metals and olefins are extremely widespread [34], and this has recently stimulated considerable interest in metal atom—olefin cryochemistry on both a matrix spectroscopic [4] and macropreparative [35] scale. Although considerable emphasis has been placed on the metal atom—olefin chemistry of the Ni, Pd and Pt [4,35] triad, not a great deal is presently known about the corresponding Co, Rh and Ir group of metals.

In this brief report, matrix synthetic and spectroscopic information for a number of new binary cobalt/ethylene complexes is presented [13]. Both mononuclear $Co(C_2H_4)_i$, binuclear $Co_2(C_2H_4)_m$ and a possible tetranuclear

$Co_x(C_2H_4)_n$ species have been reasonably well characterized from these studies; their convergence behaviour towards C_2H_{4ads} is scrutinized and discussed. Comparisons between these cobalt species [13] and the recently-reported nickel analogs [14] have proven to be particularly enlightening in terms of analyzing vibrational and electronic spectral trends, and for cross-checking earlier stoichiometric, structural and spectral assignments.
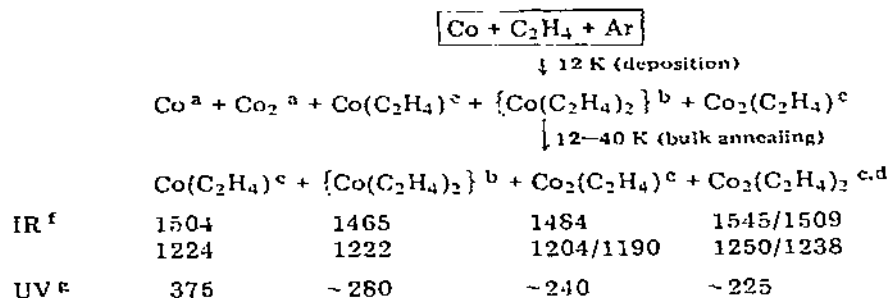
In comparison to the nickel atom—ethylene system [14], the cobalt atom/ethylene system appeared at first somewhat confusing, due to the facile matrix aggregation of atomic cobalt [10] as opposed to that of nickel [11] and the prevalent overlap complications of $\nu C=C$ and δCH_2 modes of a number of the cobalt/ethylene complexes. These were only discernible with the aid of $^{12}C_2H_4/^{13}C_2H_4$ mixed-isotope substitution and careful concentration and bulk annealing experiments. The end result of an extensive series of experiments is therefore summarized in Schemes I and II. Some representative infrared and UV—visible spectra are shown in Figs. 6—9, which have self-explanatory captions.

Evidence from the infrared spectra in pure C_2H_4 and C_2H_4/Ar matrices demonstrates that it is possible to synthesize *two* mononuclear $Co(C_2H_4)_{1,2}$ and *two* binuclear $Co_2(C_2H_4)_{1,2}$ binary cobalt-π-ethylene complexes with the following structures
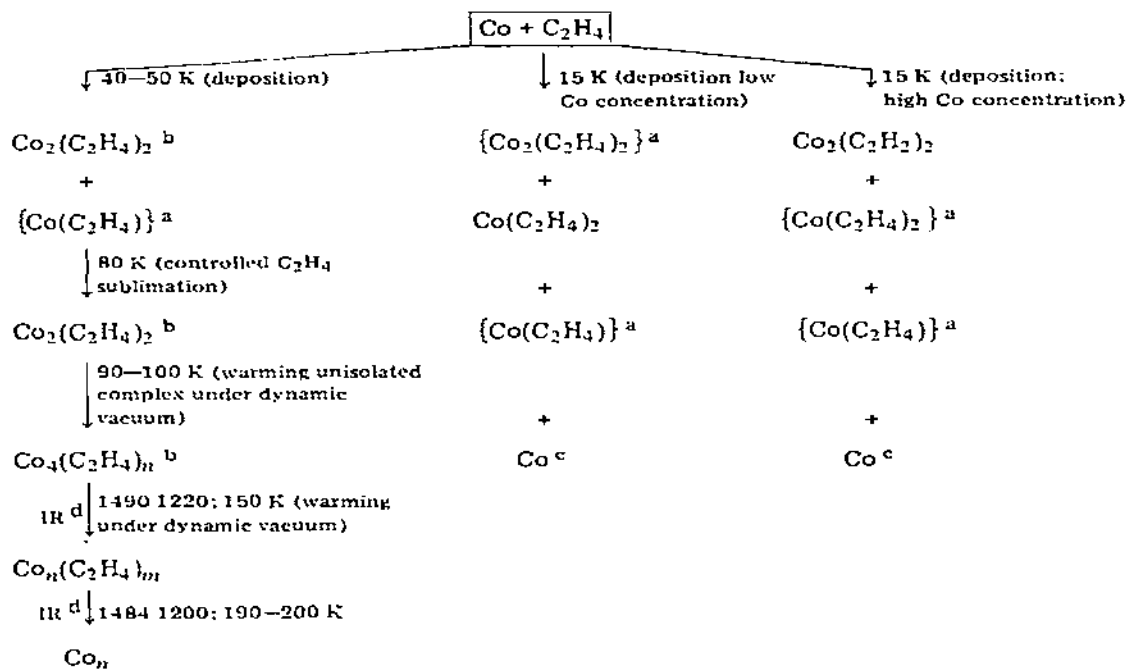
Co—‖   ‖—Co—‖   ‖—Co—Co   ‖—Co—Co—‖
(I)   (II)   (I')   (II')
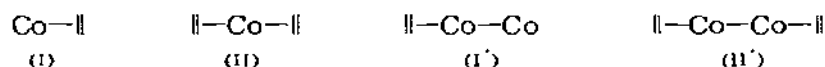
In the context of the proposed dimerization $2\ Co(C_2H_4) \rightarrow Co_2(C_2H_4)_2$ it is interesting to consider the reactions that have been discovered on controlled ethylene sublimation from a pure ethylene matrix containing mainly Co_2-$(C_2H_4)_2$. After a cobalt atom deposition with pure C_2H_4 at $1/10^4$ ratios and

Scheme I. Dilute matrices.

$$\boxed{Co + C_2H_4 + Ar}$$

$\downarrow$ 12 K (deposition)

$Co^a + Co_2{}^a + Co(C_2H_4)^c + \{Co(C_2H_4)_2\}^b + Co_2(C_2H_4)^c$

$\downarrow$ 12—40 K (bulk annealing)

$Co(C_2H_4)^c + \{Co(C_2H_4)_2\}^b + Co_2(C_2H_4)^c + Co_2(C_2H_4)_2{}^{c,d}$

IR [f]	1504	1465	1484	1545/1509
	1224	1222	1204/1190	1250/1238
UV [g]	375	~280	~240	~225

[a] Seen in the UV—visible (ref. 13 and Figs. 10 and 11). [b] Seen in the 1/20—1/50 range; highly dependent on deposition conditions. No isotopic confirmation (see ref. 13). [c] $^{12}C_2H_4/^{13}C_2H_4/(Ar)$ isotopic confirmation. [d] Predominates at high Co concentrations and after 35-K bulk annealing experiments. [e] { } braces indicate minor products under these reaction conditions. [f] In cm^{-1}. [g] In nm.

132

Scheme II. Pure ethylene matrices.

$$\boxed{Co + C_2H_4}$$

40—50 K (deposition)	15 K (deposition low Co concentration)	15 K (deposition: high Co concentration)
$Co_2(C_2H_4)_2$ [b]	$\{Co_2(C_2H_4)_2\}$ [a]	$Co_2(C_2H_2)_2$
+	+	+
$\{Co(C_2H_4)\}$ [a]	$Co(C_2H_4)_2$	$\{Co(C_2H_4)_2\}$ [a]

↓ 80 K (controlled C_2H_4 sublimation)

| $Co_2(C_2H_4)_2$ [b] | + | + |
| | $\{Co(C_2H_4)\}$ [a] | $\{Co(C_2H_4)\}$ [a] |

↓ 90—100 K (warming unisolated complex under dynamic vacuum)

| $Co_4(C_2H_4)_n$ [b] | Co [c] | Co [c] |

IR [d] ↓ 1490 1220: 150 K (warming under dynamic vacuum)

$Co_n(C_2H_4)_m$

IR [d] ↓ 1484 1200: 190—200 K

Co_n

---

[a] { } braces indicate minor products under these reaction conditions. [b] $^{12}C_2H_4/^{13}C_2H_4$ isotopic confirmation. [c] Seen in the UV—visible spectrum. [d] In cm^{-1}.

40—50 K, II' is the dominant product with a trace of II (see Figs. 8C and 9A). When the matrix is slowly warmed to 75—80 K, II' is the only detectable product after the C_2H_4 matrix support is allowed to slowly sublime away into the vacuum system. A remarkable spectral transformation is observed on allowing II' (adhering to the low-temperature optical window) in its "non-isolated" state to slowly warm to 90—100 K under dynamic vacuum conditions. The molecular conversion of II' to a new species I" (illustrated in Fig. 9A, B) was complete by 160 K.

In view of the spectral transformation of II' to I" and the suggested monoethylene stoichiometry for I" ($^{12}C_2H_4/^{13}C_2H_4$ studies), we are tempted to speculate that the dimerization reaction

$$Co_2(C_2H_4)_2 \rightarrow Co_4(C_2H_4)_4$$
$$\text{(II')} \qquad\qquad \text{(I'')}$$
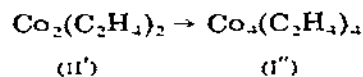
has occurred, probably with I" adopting a pseudo-tetrahedral structure
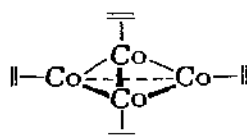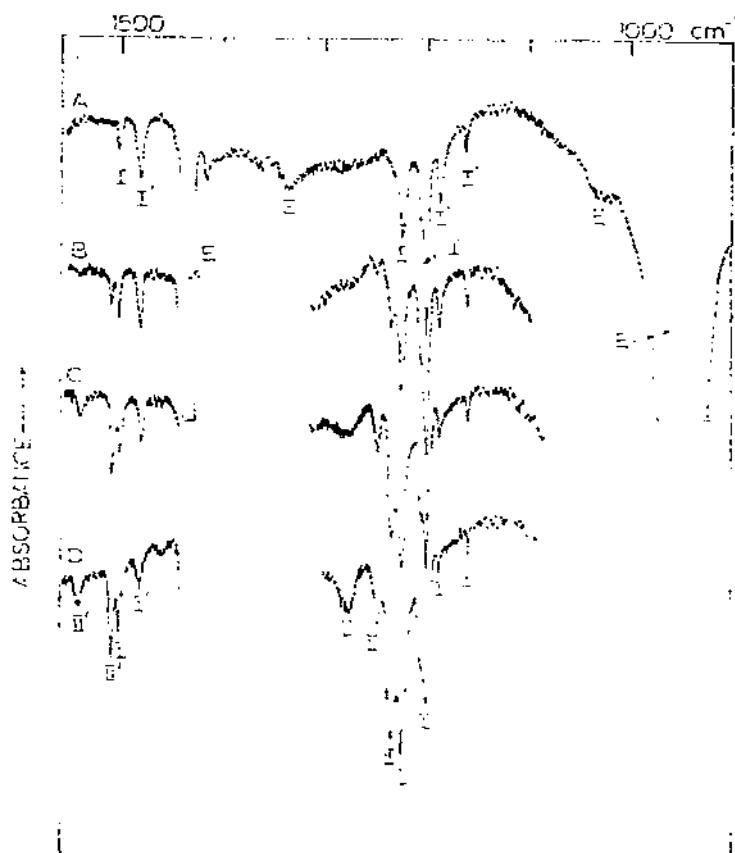
Fig. 6. The matrix-infrared spectrum of Co atoms deposited with $^{12}C_2H_4/Ar \simeq 1/50$ mixtures, with Co/Ar $\simeq 1/10^3$, at: (A) 12 K, (B)—(D) after warming to 25, 35, and 40 K, respectively, and recooling to 12 K for spectral recording. (E) refers to unreacted $^{12}C_2H_4$ in the matrix, and I = Co(C$_2$H$_4$), I' = Co$_2$(C$_2$H$_4$) and II' = Co$_2$(C$_2$H$_4$)$_2$ (ref. 13).

and with minimal vibrational coupling between the coordinated ethylenes [36].

The loss of signal for I″ at 190—200 K could represent the cluster decomposition reaction $mCo_4(C_2H_4)_n \rightarrow 4 Co_m + nmC_2H_4$, analogous to the decomposition observed [15] for $Cu_2(C_2H_4)_n$.

Examination of the optical spectra of cobalt atoms deposited into dilute C$_2$H$_4$/Ar mixtures at 12 K always shows the presence of dominant cobalt atom absorptions. Atomic Co can be seen even in a matrix with C$_2$H$_4$/Ar $\simeq 1/10$ after deposition at 12 K (see Fig. 10A, and compare with Co/Co$_2$/Ar shown in Fig. 1A, B). Under these conditions the infrared spectrum shows mainly I, I′ and a trace of II. Matrix annealing to 25 K reveals the growth of a molecular absorption at 375 nm ascribed to I (Fig. 10B) in the presence of the atomic cobalt absorptions. Further annealing to 30 K induces collapse of the
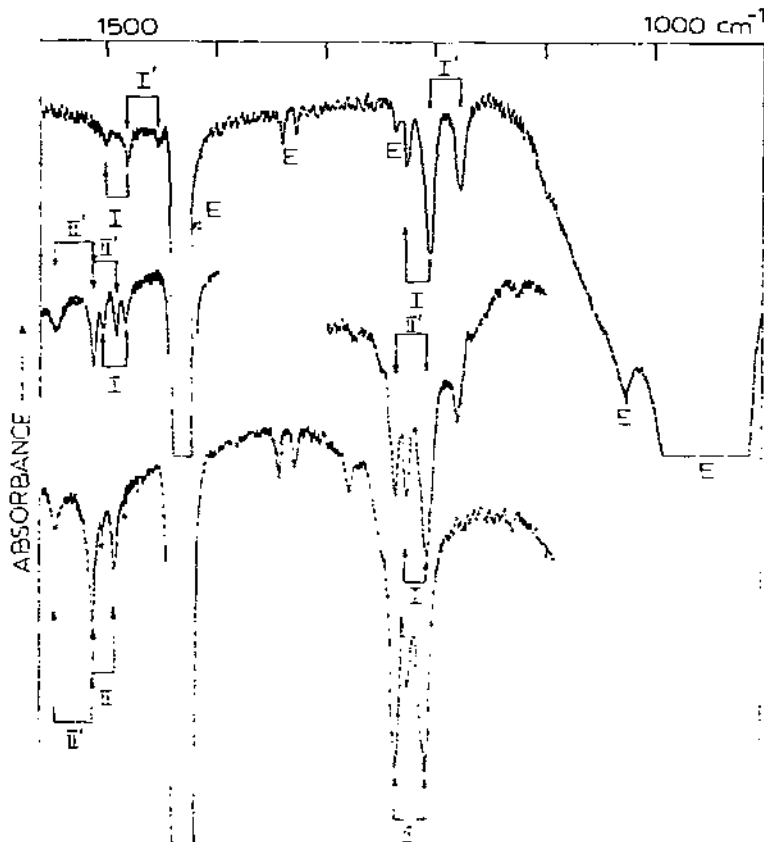
Fig. 7. Similar experiments to those illustrated in Fig. 6, except that $^{12}C_2H_4/^{13}C_2H_4/Ar$ $\simeq$ 1/1/50 mixtures were used (ref. 13).

atomic cobalt spectrum and the exposure of a new broad absorption centred around 240 nm and ascribed to I' (Fig. 10C). The choice of assignments for I and I' was based on a series of Co/C$_2$H$_4$/Ar concentration and bulk annealing experiments, with close reference to the corresponding infrared observations. The breadth of the 240-nm I' absorption was shown to arise from an overlap with the absorption due to II (280 nm) which is expected to be present under these conditions. The assignments for I and I' at 375 and 240 nm seem quite reasonable in view of the similar trend [14] observed for Ni(C$_2$H$_4$), 320 nm/Ni$_2$(C$_2$H$_4$), 240 nm; and for Cu(C$_2$H$_4$), 382 nm/Cu$_2$-(C$_2$H$_4$)$_n$, 240 nm (see Table 5).

Aside from some inhomogeneous band-broadening effects and loss of fine structural detail, the spectra of atomic Co in mixtures with C$_2$H$_4$/Ar $\simeq$ 1/10 are essentially identical to those observed for pure argon matrices. The absence of Co$_2$ in Fig. 10 (parts A and B) is noteworthy in that it implies the main
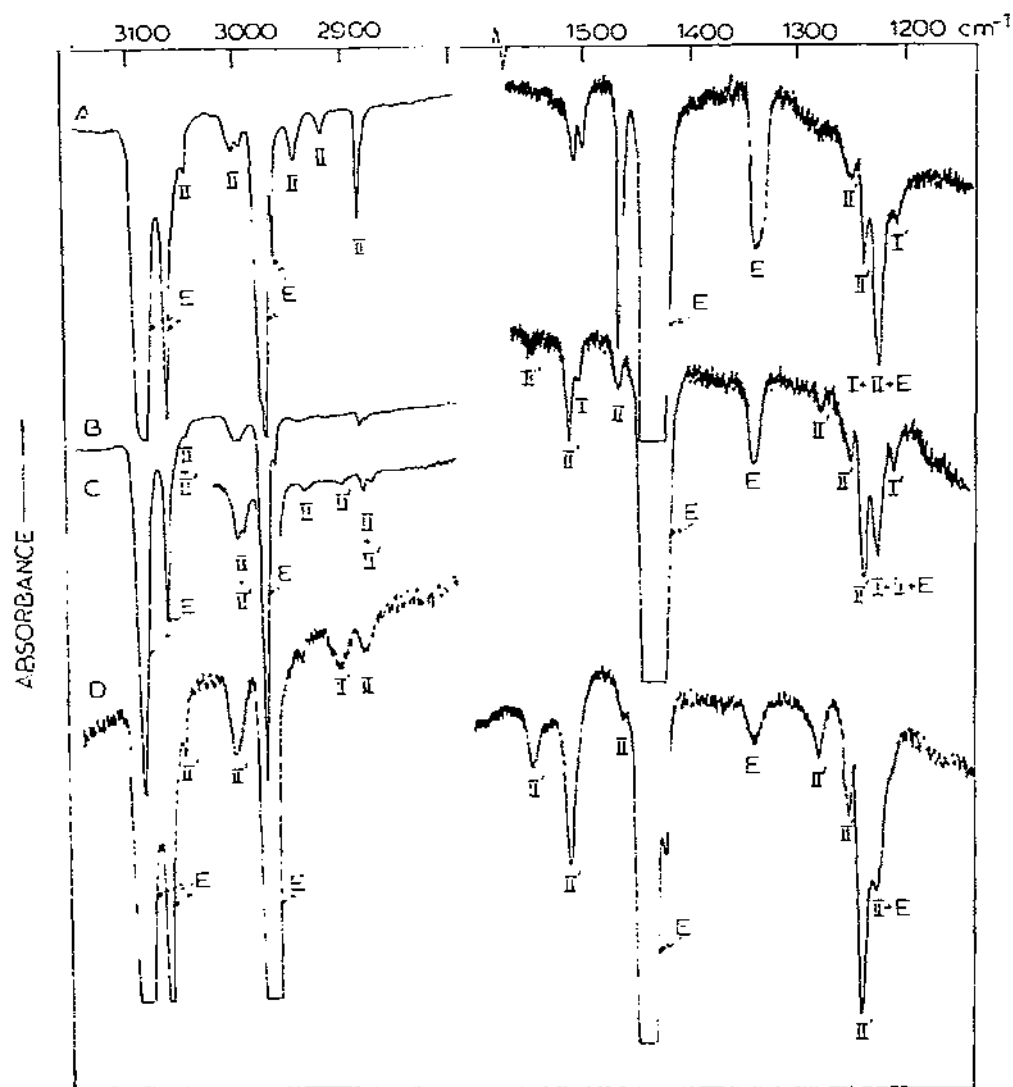
Fig. 8. The matrix-infrared spectrum of Co atoms deposited with $^{12}C_2H_4$ at 12 K, with (A) $Co/C_2H_4 \simeq 1/10^4$, (B) $Co/C_2H_4 \simeq 1/10^3$; (C) deposited at 40—50 K with $Co/C_2H_4 \simeq 1/10^4$. (E) refers to unreacted ethylene, and I = $Co(C_2H_4)$, I' = $Co_2(C_2H_4)$, II = $Co(C_2H_4)_2$ and II' = $Co_2(C_2H_4)_2$ (ref. 13).

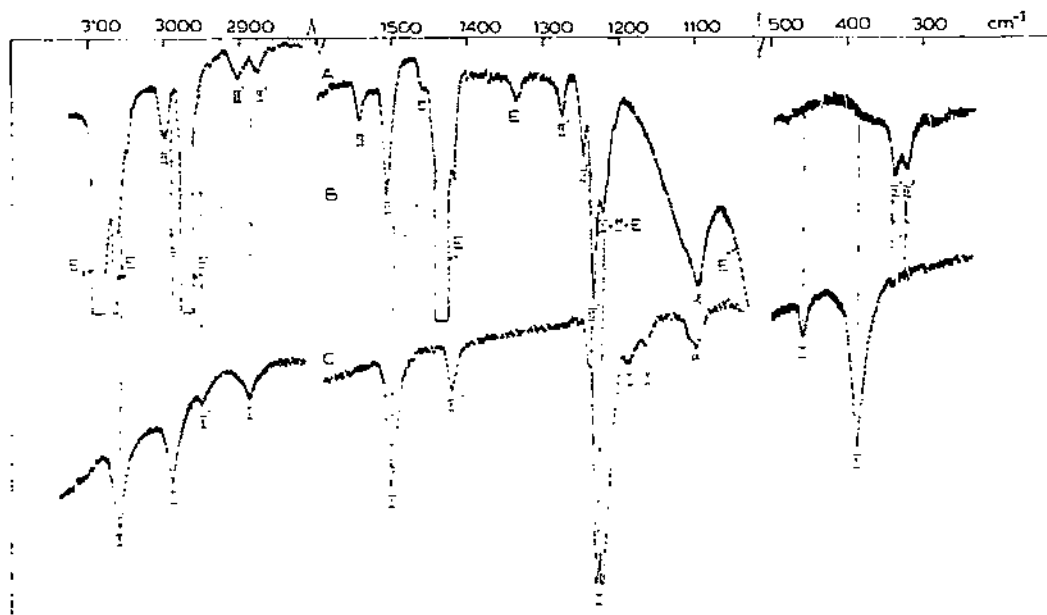pathway to I' is via route k_1'' rather than k_1' in the following reaction network
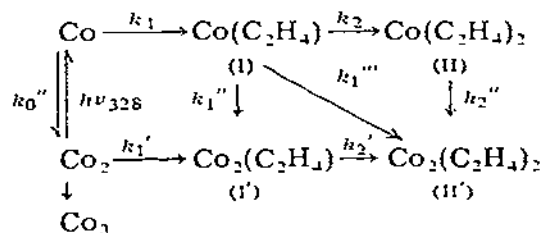
Fig. 9. (A) The same spectrum as shown in Fig. 8C; (B) the same spectrum as Fig. 8C, but using 91% $^{13}C_2H_4$; (C) the spectrum obtained after controlled $^{12}C_2H_4$ sublimation at 75—80 K from the matrix in (A) and further warming to 90—100 K, showing the transformation of II' = $Co_2(C_2H_4)_2$ to I" = $Co_4(C_2H_4)_n$ (ref. 13).

The generation of detectable quantities of Co_2 in the presence of Co becomes apparent in matrices with $C_2H_4/Ar \simeq 1/50$, an example of which is shown in Fig. 11A. Considerable insight into the competing diffusion-reaction processes occurring in these mixtures can be obtained by surveying the UV—visible spectral alterations which ensue in these 1/50 matrices during 12—40-K bulk annealing experiments (Fig. 11B, C). In essence, atomic Co is consumed rapidly (compared to identical experiments in pure Ar matrices [10]) and Co_2 maintains an approximately steady-state concentration up to about 35 K and then gradually decays around 40 K, at which temperature detectable amounts of Co_3 (316, 287 nm) [10] and $Co_2(C_2H_4)$ (I') begin to appear. Under these conditions, the expected formation of I (375 nm) would be obscured by the intense low-energy absorption of Co_2. Although interesting, these observations cannot be used to distinguish between pathways k_1' or k_1'' as the route to I'. Clearly competing cobalt atom aggregation reactions accompany Co/C_2H_4 complexation under dilute conditions ($C_2H_4/Ar \simeq 1/50$), whilst under 1/10 conditions these nucleation events are more efficiently quenched.

Having realized that substantial concentrations of atomic cobalt can be isolated even in concentrated C_2H_4/Ar mixtures at 12 K, pointing to the existence of a small yet finite activation energy for Co/C_2H_4 complexation, it was not too surprising to discover that atomic cobalt could also be isolated in

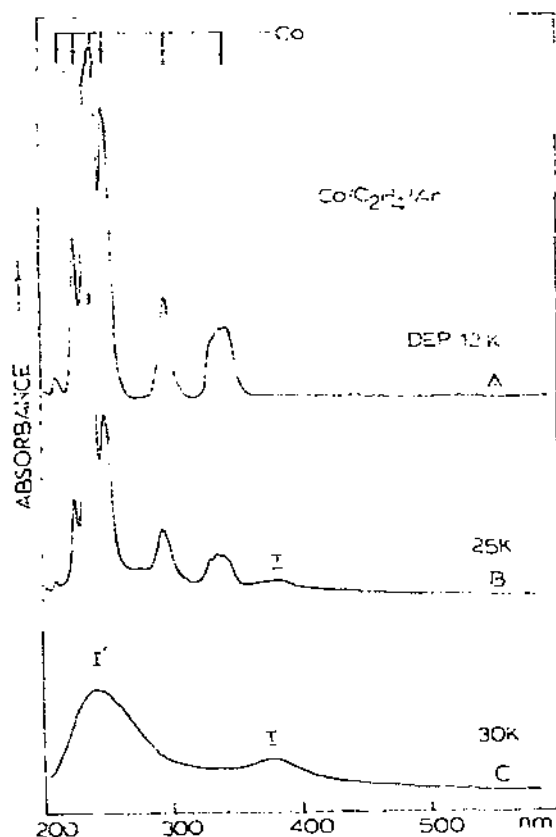Fig. 10. The ultraviolet—visible spectra obtained on co-depositing Co atoms with C_2H_4/Ar $\simeq 1/10$ mixtures so that $Co/Ar \simeq 1/10^4$; (A) at 12 K; (B) and (C) after warm-up to 25 and 30 K, respectively, and recooling to 12 K for recording purposes (ref. 13).

TABLE 4

Infrared spectral data for $M(C_2H_4)_m$ and $M_2(C_2H_4)_m$ (where M = Co, Ni, $m = 1$ or 2) in the $\nu C=C$ and δCH_2 regions

	Co [a] (cm^{-1})	Ni [a] (cm^{-1})	Assignment
$M(C_2H_4)$	1504	1490	$\nu C=C$
	1224	1160	δCH_2
$M(C_2H_4)_2$	1465	1465	$\nu C=C$
	1222	1223	δCH_2
$M_2(C_2H_4)$	1484	1488	$\nu C=C$
	1204/1190	1208/1180	δCH_2
$M_2(C_2H_4)_2$	1545/1509	1504	$\nu C=C$
	1276/1250/1238	1232	δCH_2

[a] νMC modes observed at 340 and 320 cm^{-1} for $Co_2(C_2H_4)_2$, and at 446 and 416 cm^{-1} for $Ni_2(C_2H_4)_{1,2}$ are in line with the greater thermal stability of the cobalt—ethylene complexes.
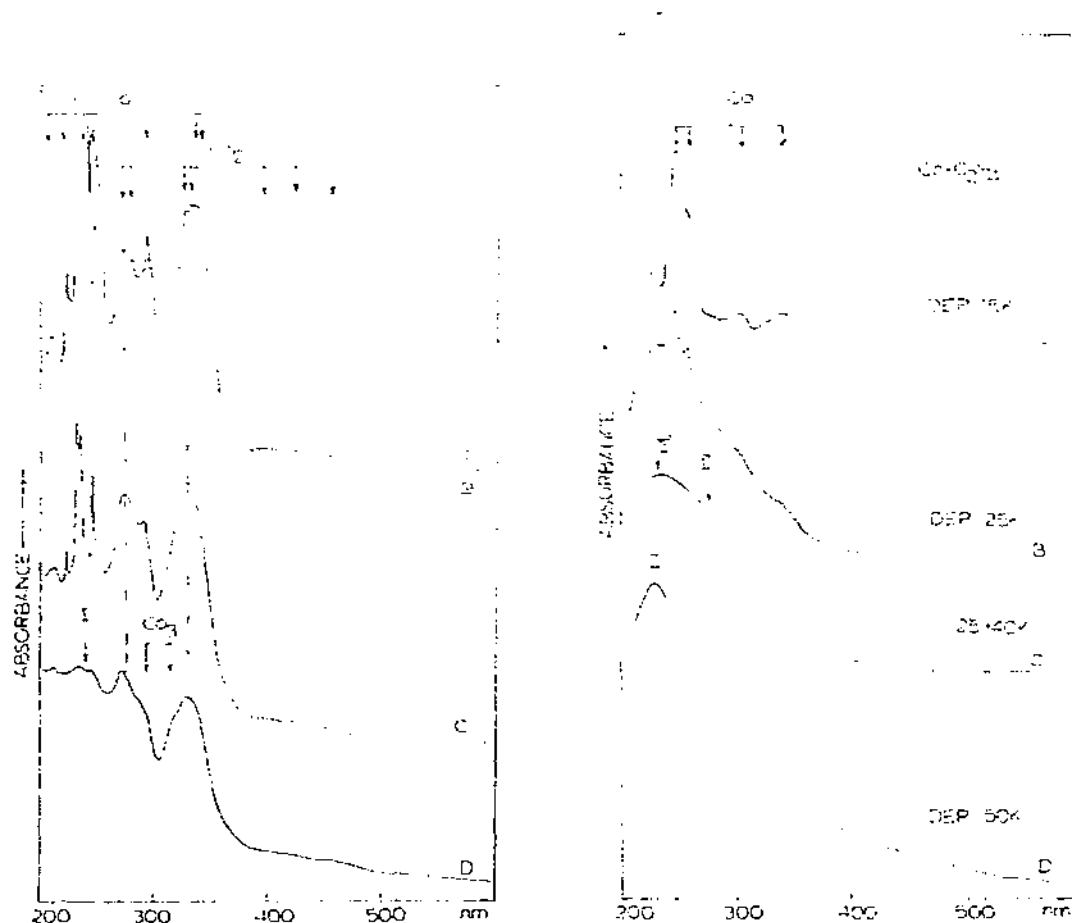
Fig. 11. The ultraviolet—visible spectra obtained on depositing Co atoms at 12 K with: (A) $C_2H_4/Ar \simeq 1/50$ mixtures, showing mainly Co and Co_2; (B) $C_2H_4/Ar \simeq 1/10$ mixtures, showing mainly Co; (C) and (D), the matrix shown in (A) after bulk annealing at 25 K and 40 K, respectively, showing the rapid consumption of Co atoms, slower loss of Co_2, and gradual appearance of Co_3 and $I' = Co_2(C_2H_4)$. Complex $I = Co(C_2H_4)$, expected to absorb weakly around 375 nm, is probably masked by the low-energy Co_3 band (ref. 13).

Fig. 12. The ultraviolet—visible spectra of the products formed when Co atoms are condensed with C_2H_4 matrices: (A) at 15 K; (B) at 25 K; (C) after warming the matrix used in (B) to 40 K and recooling to 12 K for spectral recording purposes; and (D) Co co-condensation at 50 K (ref. 13).

mixtures with $Co/C_2H_4 \simeq 1/10^3$ at 12—15 K (Fig. 12A). Remember that under these conditions compound formation has occurred, as indicated by the infrared observation that mainly II and II' are present (Fig. 8 and Scheme II). This implies that the UV molar absorbances of unreacted Co atoms under these deposition conditions must greatly outweigh and/or overlap with those associated with II and II'. By gradually increasing the deposition temperature

TABLE 5

Ultraviolet spectral data [a] for $M(C_2H_4)_m$ and $M_2(C_2H_4)_m$ (where M = Co, Ni, or Cu, m = 1 or 2)

Complex	Co [13]	Ni [14,38]	Cu [15]
$M(C_2H_4)$	375	320	382
$M(C_2H_4)_2$	~280 [b]	280	276
$M_2(C_2H_4)$	240	{ 240	{ 240
$M_2(C_2H_4)_2$	225		

[a] In nm.
[b] Appears as a broad shoulder on the 240-nm absorption of $Co_2(C_2H_4)$.

from 12—15 K to 25 K and to 50 K, the delicate kinetic balance which must exist between isolating (i) *only* Co atoms, (ii) Co atoms *and* Co/C_2H_4 complexes and (iii) *only* Co/C_2H_4 complexes, can be monitored and analyzed in terms of overlapping absorptions of II at ~280 nm and II' at ~225 nm (see Fig. 12A—D and Table 5). Collected together in Table 5, the optical assignments for both $M(C_2H_4)_{1,2}$ and $M_2(C_2H_4)_{1,2}$ (where M = Co, Ni, Cu) appear to form a reasonable set.

D. ELECTRONIC AND VIBRATIONAL SPECTRA

In the cobalt/ethylene system, as now seems to be universal in binary transition metal-π-ethylene complexes, the "mainly intraligand" infrared modes are relatively insensitive to both ethylene stoichiometry and metal cluster size. However, this does not seem to be quite the case for the metal—ligand stretch-

TABLE 6

Comparison of HREELS for C_2H_4 on Ni(111) with $Ni_n(C_2H_4)$ chemisorption models

HREELS [e] C_2H_4/Ni(111) [37]	$Ni(C_2H_4)$ Ar/10 K [38]	$Ni_2(C_2H_4)$ Ar/10 K [14]	Assignment
2940	2963	2880, 2908	νCH_2
2690 [c]			νCH_2 [c]
1500 [a]	1499	1488	$\nu C=C$
1430	[b]	[b]	δCH_2
1090	1160	1208, 1180	$\rho_w CH_2$
880	902	910	$\rho_r CH_2$
440	376	416 or 446 [d]	νNiC

[a] Weak band observed around 1500 cm^{-1}; this could be a surface-dipole-forbidden $\nu C=C$ mode. [b] Hidden under intense δCH_2 mode of free C_2H_4 in the matrix. [c] Softened νCH_2 surface mode. [d] One of these bands belongs to $Ni_2(C_2H_4)_2$. [e] HREELS = High Resolution Electron Energy Loss Spectroscopy.

TABLE 7

Comparison of HREELS for C_2H_4 on Ni(111) with $Co_n(C_2H_4)_m$ chemisorption models

HREELS C_2H_4/Ni(111) [37]	$Co_2(C_2H_4)_2$ [13]	$Co_4(C_2H_4)_n$ [13]	Assignments [a]
	3048wsh	3057s	
2940	3000m	2984s	νCH_2
	2900m	2948w	
	2876w	2888wbr	
2690	—	—	νCH_2 [b]
1500	1544w/1508s	1469/1492s	$\nu C=C$
1430	1420w	1416w	δCH_2
1090	1276w/1248w/1234s	1224/1216s	$\rho_w CH_2$
880	—	—	$\rho_r CH_2$
440	332w	460w	$\nu M-C$
	314w	384s	

[a] The paper by J.P. Sorzano and J.P. Fackler Jr. [J. Mol. Spectrosc., 22 (1967) 80] is a useful reference source for detailed vibrational—normal coordinate studies of coordinated C_2H_4. [b] Softened mode.

ing modes so far observed for the nickel— and cobalt—ethylene systems (see Tables 4, 6 and 7). For example, on passing from Ni(C_2H_4) to Ni$_3(C_2H_4)_{1,2}$, the observed νNi—C stretching modes shift from 376 cm^{-1} to 416 and 446 cm^{-1}, respectively. In the case of $Co_2(C_2H_4)_2$ and $Co_4(C_2H_4)_n$, the observed νCo—C modes shift from 332 and 314 cm^{-1} to 384 and 460 cm^{-1}, respectively. The point to notice here is the reasonably high sensitivity of the νM—C modes to both metal cluster size and the nature of the metal. The higher νM—C energies observed for the nickel complexes relative to the cobalt complexes are in line with the correspondingly greater thermal stabilities of the former compared to the latter; this property would probably be manifested in the adsorption energies for chemisorbed ethylene on Ni and Co surfaces (which, as far as we are aware, have not yet been reported in the literature) and probably reflects on the superior hydroformylation catalytic properties of cobalt relative to nickel.

On surveying the available data in Tables 4, 6, 7 for Co(C_2H_4)/Co$_2$-(C_2H_4)$_{1,2}$/Co$_4(C_2H_4)_n$ and Ni(C_2H_4)/Ni$_3(C_2H_4)_{1,2}$, one can make certain useful statements about the suitability of finite cluster—ethylene complexes as localized bonding models for chemisorbed ethylene. Apart from the rather special νCH_2 "softened mode" at 2690 cm^{-1} (a surface hydrogen bonding interaction in the terminology of Demuth et al. [37]), the νCH_2 region of so-called π-chemisorbed ethylene on Ni(111) is dominated by a broad vibrational loss around 2940 cm^{-1} (see Table 6). Clearly this band "envelope" corresponds to bands observed in the 3050—2875 cm^{-1} region of our finite cluster ethylene complexes. Significantly, the crucial νC=C stretching modes of ethylene π-bonded to the surface metal atom sites and π-bonded in our

complexes are relatively insensitive to cluster size or ethylene stoichiometry, being observed as a weak band around 1500 cm^{-1} (surface selection rule arguments) on the Ni(111) surface and around 1504 (I), 1484 (I'), 1508 (II'), and 1494 (I'') cm^{-1} for the cobalt complexes and 1499 (I), 1488 (I') and 1504 (II') cm^{-1} for the nickel complexes [14] (Tables 6 and 7). The observed δCH_2 deformational modes in the 1400- and 1200-cm^{-1} regions also seem to be relatively insensitive to cluster size and the nature of the metal, although the 1200-cm^{-1} group of bands are shifted by roughly 100 cm^{-1} with respect to the corresponding surface modes (Table 6).

It would seem, therefore, that the δCH_2 modes around 1200 cm^{-1} and the $\nu M-C$ modes around 300–450 cm^{-1} are likely to be most informative in terms of localized bonding discussions. In particular, it would appear that increasing the cluster size from $1 \rightarrow 2 \rightarrow 4$ causes a monotonic *blue* shift of $\nu M-C$ towards the value observed for the corresponding surface—ethylene chemisorption mode, being already reasonably close for 2 to 4 metal-atom clusters. Broadly speaking, one can reasonably conclude that it is possible to represent π-chemisorbed ethylene by a finite cluster—ethylene complex containing as few as 2 to 4 metal atoms in the case of Co and Ni.

In spite of the general insensitivity of the intraligand vibrational modes to cluster size, there are a few specifics worth mentioning, particularly with respect to the trends in $\nu C=C$. The first point relates to the observed $\nu C=C$ orderings.

$$Co(C_2H_2) > Co(C_2H_4)_2$$

$$Ni(C_2H_4)_3 > Ni(C_2H_4) > Ni(C_2H_4)_2$$

$$Cu(C_2H_4)_3 > Cu(C_2H_4)_2 > Cu(C_2H_4)$$
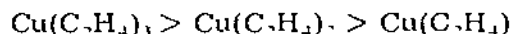
The amonotonic order for cobalt and nickel compared to the monotonic order for copper mononuclear ethylene complexes (like earlier discussions [38] on M(CO)$_n$ can best be rationalized in terms of a finite positive interaction force constant, $k_{C=C \cdot C=C}$, for Co and Ni rather than as the outcome of amonotonicity in the principal stretching force constants, $k_{C=C}$.

At this point it is significant to note that $\nu C=C$ (or $k_{C=C}$) for M(C$_2$H$_4$) complexes adopts the following order

$$Co(C_2H_4) \quad > \quad Ni(C_2H_4) \quad > \quad Cu(C_2H_4)$$
$$(1509 \text{ cm}^{-1}) \quad (1496 \text{ cm}^{-1}) \quad (1475 \text{ cm}^{-1})$$
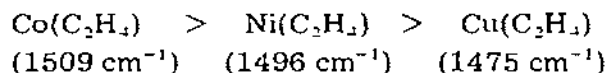
If we accept the GVB—CI conclusion [14] that the nickel atom in Ni(C$_2$H$_4$) adopts the $s^1 d^9$ electronic configuration with a major $\pi(C_2H_4) \rightarrow \sigma(sp)$Ni donor yet a minimal $\pi^*(C_2H_4) \leftarrow d_\pi$(Ni) acceptor interaction, then we would predict that the monotonic $\sigma(sp)/d_\pi$ metal orbital variations illustrated in Fig. 13 would hold true on passing from $(s^1 d^8)$Co to $(s^1 d^9)$Ni and to $(s^1 d^{10})$Cu. Thus, for a dominant $\pi(C_2H_4) \rightarrow \sigma(sp)$M bonding interaction one would expect the strongest metal—ethylene bond to occur for Cu and the weakest
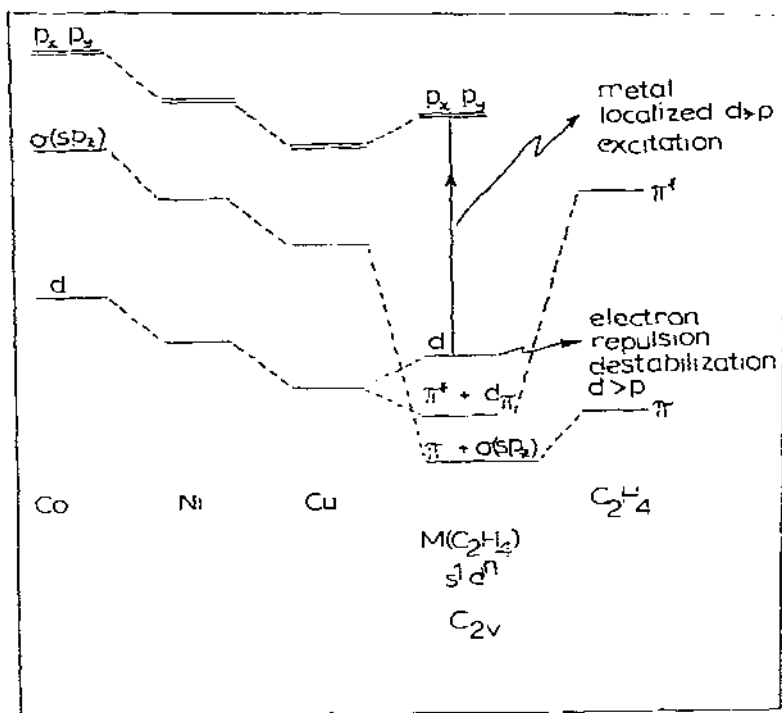
Fig. 13. Schematic representation of the $\sigma(sp_z)$, $p_{x,y}$ and d metal-orbital energy variations on passing from Co to Ni to Cu in C_{2v} $M(C_2H_4)$ π-ethylene complexes (ref. 13).

for Co in $M(C_2H_4)$ complexes. This would be consistent with the *highest* $\nu C{=}C$ for $Co(C_2H_4)$ and the $\nu C{=}C$ ordering Co > Ni > Cu. Such a rationale would not be expected to hold true for the bis- and tris(ethylene) complexes as the electronic configuration of the metal is likely to move away from s^1d^8/s^1d^9 in $Co(C_2H_4)/Ni(C_2H_4)$ to p^1d^8/p^1d^9 or d^9/d^{10} in $Co(C_2H_4)_{2,3}/Ni(C_2H_4)_{2,3}$ and from s^1d^{10} in $Cu(C_2H_4)$ to p^1d^{10} in $Cu(C_2H_4)_{2,3}$ (in line with ESR evidence for $Cu(C_2H_2)_{1,2}$) [39].

Some other fascinating parallels in the $\nu C{=}C$ frequencies worthy of consideration are as follows

Co—‖
1504 cm⁻¹
(C_{2v})

Ni—‖
1499 cm⁻¹
(C_{2v})

Co—Co—‖
1484 cm⁻¹
(C_{2v})

Ni—Ni—‖
1488 cm⁻¹
(C_{2v})

‖—Co—Co—‖
1508 cm⁻¹

‖—Ni—Ni—‖
1504 cm⁻¹

To begin with, we note a roughly constant difference of 4—5 cm^{-1} on passing from $M(C_2H_4)$ to its dimer, $M_2(C_2H_4)_2$. Secondly, the $\nu C=C$ frequencies first *red* shift on passing from $M(C_2H_4)$ to $M_2(C_2H_4)$ and then *blue* shift from $M_2(C_2H_4)$ to $M_2(C_2H_4)_2$.

Within the GVB—CI description [14] of the bonding interactions in $M(C_2H_4)$, we note that on adding the second metal in an s^1d^n promoted (valence) state (which is very close in energy to the s^2d^n repulsive ground state) to the s^1d^n metal atom in $M(C_2H_4)$, the repulsive interaction between the charge density in the $\sigma(sp)$-non-bonding orbital and the π-charge density of the incoming ethylene ligand in $M(C_2H_4)$ is *reduced* slightly in $M_2(C_2H_4)$ [14]. In other words, the (sp)-charge density is polarized more away from the ethylene in $M_2(C_2H_4)$ than in $M(C_2H_4)$ [14]. The outcome is a closer approach of the ethylene to the metal atom site in $M_2(C_2H_4)$ than in $M(C_2H_4)$, resulting in a greater delocalization of charge from the π-orbital of the ethylene onto the metal site in $M_2(C_2H_4)$ and hence a *lower* $\nu C=C$ frequency with respect to $M(C_2H_4)$.

The subsequent *blue* shift in the $\nu C=C$ stretching frequency on passing from $M_2(C_2H_4)$ to $M_2(C_2H_4)_2$ probably arises from increased charge repulsion effects between the π-electron densities of the ethylenes and the mainly s—s charge density localized in the metal—metal bond. One therefore anticipates a weaker $\pi(C_2H_4) + \sigma(sp)M$ bonding interaction in $M_2(C_2H_4)_2$ which is manifested in a *blue* $\nu C=C$ shift with respect to $M_2(C_2H_4)$. Finally, we note in passing that the detection of two $\nu C=C$ stretching modes for $Co_2(C_2H_4)_2$ (sym $\nu C=C$, 1545 cm^{-1}; asym $\nu C=C$, 1508 cm^{-1}) necessitates a non-centrosymmetric geometry. The observation of a single $\nu C=C$ value for $Ni_2(C_2H_4)_2$ suggests that the geometry is either centrosymmetric or that it is non-centrosymmetric but that the symmetric $\nu C=C$ mode has remained undetected. This distinction, if real, could conceivably be a reflection of stabilization differences necessitated by an s^1d^8 cobalt atom in $Co_2(C_2H_4)_2$ relative to an s^1d^9 nickel atom in $Ni_2(C_2H_4)_2$.

The discussion of $d_\pi/\sigma(sp)$ orbital trends for the $M(C_2H_4)$ complexes leads us to the interesting ordering of observed UV transition energies

$$Co(C_2H_4) < Ni(C_2H_4) > Cu(C_2H_4)$$

$$(375\ nm)\quad (320\ nm)\quad (382\ nm)$$
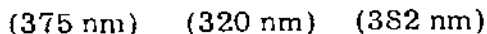
If we accept the GVB—CI assignment for the 320-nm UV transition of $Ni(C_2H_4)$ in terms of a $d \to p$ excitation, localized on an s^1d^9 nickel atom [14] (in line with recent UV studies of Ni(olefin) complexes for a wide variety of substituted olefins [40]), then one has to account for a metal localized $d \to p$ energy ordering in $M(C_2H_4)$ of the form Co < Ni > Cu. In terms of free-atom effective nuclear charge/orbital penetration arguments, one would initially expect the $d \to p$ energy gap to follow the order Co < Ni < Cu. Clearly this is an

144

oversimplified explanation and account must be taken of the effect of a monotonically-increasing $\pi(C_2H_4) \to \sigma(sp)M$ charge donation from ethylene to the metal in $M(C_2H_4)$. This will clearly have the opposite effect to Z^*/penetration effects alone and could well account for the "anomalously" low energy of the $d \to p$ excitation observed for $Cu(C_2H_4)$ and the resulting amonotonic $d \to p$ metal localized ordering, Co < Ni > Cu. This intriguing point will hopefully be scrutinized in future ab initio CI molecular orbital calculations of $M(C_2H_4)$ systems. It will be fascinating to discover whether the corresponding UV surface excitations anticipated for $M(C_2H_{4ads})$, possibly observable by HREELS techniques of the type recently reported by Rubloff [41] for CO on Ni(111), will display a parallel energy trend to that observed for $M(C_2H_4)$.

REFERENCES

1 See for example, International Meeting on Small Particles and Inorganic Clusters, J. Phys. Paris, Colloq., C-2 (1977), and refs. therein.
2 F.F. Abraham, Homogeneous Nucleation Theory, Academic Press, New York, N.Y., 1974.
3 (a) J.F. Hamilton, J. Vac. Sci. Technol., 13 (1976) 319; (b) R.C. Baetzold, J. Appl. Phys., 47 (1976) 3799; (c) J.F. Hamilton and P.C. Logel, Photogr. Sci. Eng., 18 (1974) 507.
4 G.A. Ozin, Acc. Chem. Res., 10 (1977) 21 and Catal. Rev. Sci. Eng., 16 (1977) 191, and refs. therein.
5 (a) R.P. Messmer, Cluster Model Theory and Its Application to Metal Surface Adsorbate Systems, in G. Ertl and T.N. Rhodin (Eds.), The Nature of the Surface Chemical Bond, North-Holland, Amsterdam 1978, and refs. therein; (b) R.P. Messmer, S.K. Knudson,

K.H. Johnson, J.B. Diamond and C.Y. Yang, Phys. Rev. B, 13 (1976) 1396, and refs. therein.

6   K.H. Johnson, A.C. Balazs and H.J. Kolari, Surf. Sci., 72 (1978) 733, and refs. therein.
7   J.H. Sinfelt, Acc. Chem. Res., 10 (1977) 15, and refs. therein.
8   M. Moskovits and G.A. Ozin (Eds.), Cryochemistry, John Wiley and Sons, New York, 1976, and refs. cited therein.
9   (a) G.A. Ozin and H. Huber, Inorg. Chem., 17 (1978) 155; (b) G.A. Ozin and W. Klotzbücher, J. Am. Chem. Soc., 100 (1978) 2262; (c) G.A. Ozin and S.A. Mitchell, J. Am. Chem. Soc., 100 (1978) 6776; (d) G.A. Ozin, Naked Cluster Cryophotochemistry, presented at the Cluster Symposium, Am. Chem. Soc. Meet., Anaheim, March, 1978; G.A. Ozin, D. McIntosh, S. Mitchell, H. Huber, J.G. Norman, Jr. and L. Noodleman, Naked Dicopper and Disilver Cryophotochemistry and SCF-Xa-SW Molecular Orbital Calculations, presented at the C.I.C. Meeting, Winnipeg, June, 1978, and submitted to Inorg. Chem.; S. Mitchell, G.A. Ozin and H. Huber, Naked Trisilver Cryptochemistry, Inorg. Chem., (1978), in press.
10 A.J. Lee Hanlan, S. Mitchell, D. McIntosh, R.P. Messmer and G.A. Ozin, in preparation.
11 J. Hulse and M. Moskovits, J. Chem. Phys., 66 (1977) 3988.
12 J. Hulse and M. Moskovits, J. Chem. Phys., 67 (1977) 4271.
13 A.J. Lee Hanlan, G.A. Ozin and W.J. Power, Inorg. Chem., 17 (1978) 3648.
14 G.A. Ozin, W.J. Power, T. Upton and W.A. Goddard III, J. Am. Chem. Soc., 100 (1978) 4750.
15 G.A. Ozin, H. Huber and D. McIntosh, Inorg. Chem., 16 (1977) 3070.
16 See for example, (a) P.W. Jolly and G. Wilke, The Organic Chemistry of Nickel, Vols. I and II, Academic Press, New York, 1974; (b) P.M. Maitlis, The Organic Chemistry of Palladium, Vols. I and II, Academic Press, New York, 1971; (c) F. Basolo and R.L. Burwell, Jr. (Eds.), Catalysis, Progress in Research, Plenum Press, London, 1973.
17 (a) G.A. Somorjai, Acc. Chem. Res., 9 (1976) 248; (b) J.C. Bucholz and G.A. Somorjai, Acc. Chem. Res., 9 (1976) 333; (c) J.T. Yates, Chem. Eng. News, Aug. 26, 1974, p. 19; (d) W.E. Spicer, I. Lindau and C.R. Helms, Res. Dev., 28 (1977) 20; (e) E. Drauglis and R.I. Jaffee (Eds.), The Physical Basis of Heterogeneous Catalysis, Plenum Press, New York, 1975.
18 D.M. Mann and H.P. Broida, J. Chem. Phys., 55 (1971) 84.
19 A. Kant and B. Strauss, J. Chem. Phys., 41 (1964) 3806.
20 W. Cooper, G.A. Clarke, T.P. Sleight and C.R. Hare, J. Phys. Chem., 76 (1972) 2268.
21 J. Hulse and M. Moskovits, J. Chem. Soc. Faraday Trans. 2, (1977) 471.
22 M. Belzons and G. Rasigni, C.R. Acad. Sci., 261 (1965) 4042; M. Belzons, C.R. Acad. Sci., 260 (1965) 4707.
23 S. Mitchell and G.A. Ozin, in preparation.
24 W. Klotzbücher and G.A. Ozin, Inorg. Chem., (1978) in press.
25 K.A. Gingerich, J. Cryst. Growth, 9 (1971) 31, and refs. cited therein.
26 B. Rosen, Spectroscopic Data Relative to Diatomic Molecules, Pergamon Press, New York, 1970, and refs. therein.
27 (a) R.C. Baetzold, J. Chem. Phys., 55 (1971) 4355; (b) A.B. Anderson, J. Chem. Phys., 68 (1978) 1744.
28 J.B. Danese, J. Chem. Phys., 61 (1974) 3071; J.B. Danese, Chem. Phys. Lett., 45 (1977) 150.
29 N. Aslund, R.F. Barrow, W.G. Richards and D.N. Travis, Ark. Fys., 30 (1965) 171.
30 B. Klemen and S. Lindkvist, Ark. Fys., 8 (1954) 333, and 9 (1955) 385.
31 The Electron Factor in Catalysis on Metals, Natl. Bur. Stand. U.S., Spec. Publ., 475 (1977), and refs. cited therein.
32 H. Ibach, H. Hopster and B. Secton, Appl. Surf. Sci., 1 (1977) 1, and refs. therein.
33 F.P. Netzer, R.A. Wille and J.A.D. Matthew, Solid State Commun., 21 (1977) 97; J. Kuppers, Surf. Sci., 36 (1973) 53; K. Christmann, O. Schober and G. Ertl, J. Chem. Phys., 60 (1974) 4719.

34 See for example, M.M. Taqui Khan and A.E. Martell, Homogeneous Catalysis by Metal Complexes, Vol. II, Academic Press, New York, 1974.

35 See for example, (a) Chapters by P.L. Timms, M. McGlinchey and P.S. Skell in M. Moskovits and G.A. Ozin (Eds.), Cryochemistry, John Wiley and Sons, New York, 1976; (b) P.L. Timms, Adv. Organomet. Chem., 15 (1977) 53; (c) K. Klabunde, Acc. Chem. Res., 8 (1975) 393, and refs. therein.

36 The vibrational data do not easily allow one to differentiate between a $Co_4(C_2H_4)_4$ formulation and lower-ethylene stoichiometry complexes formed in a disproportionation reaction such as

$$2 Co_2(C_2H_4)_2 \rightarrow Co_4(C_2H_4)_n + (4-n)C_2H_4.$$

37 J. Demuth, H. Ibach and S. Lehwald, Surf. Sci., in press; J. Demuth, personal communication.

38 H. Huber, G.A. Ozin and W.J. Power, J. Am. Chem. Soc., 98 (1976) 6508.

39 P. Kasai J. Am. Chem. Soc., 100 (1978) 625.

40 G.A. Ozin and W.J. Power, Inorg. Chem., 17 (1978) 2836.

41 G. Rubloff, IBM Report, personal communication.

42 C.M. Brown and M.L. Ginter, J. Mol. Spectrosc., 69 (1978) 25.

43 W. Klotzbücher and G.A. Ozin, Photoselective Bimetallic Aggregation: a New Route to Bimetallic Clusters, Proc. Mater. Res. Symp., Characterization of High Temperature Vapors and Gases, 10th, Natl. Bur. Stand. U.S., Spec. Rep., (1978), and J. Am. Chem. Soc., 100 (1978) 2262.

44 Recent emission experiments by Kolb and Leutleff [45a] and Ozin et al. [45c], employing 300—330 nm excitation of Ag atoms in inert gas matrices, have revealed the presence of several intense emission bands. In the case of Ar and Kr the largest Stokes shift corresponds to the most intense band which is centered in the 400—500-nm region. The large Stokes shift suggests the existence of a significant non-radiative energy channel following Ag-atom photoexcitation, of which the observed metal-atom photomobility is presumably a manifestation. We suggest the following simplified scheme (Scheme A) which seems most consistent with the available experimental information. This scheme represents a qualitative model to explain both the photomobilization and emission which occurs following 300-nm excitation of matrix-entrapped Ag atoms. However, future studies [45c] on the time-dependence and polarization of the emissions may well reveal a more complex mechanism.
Scheme A
(i) ground-state $^2S_{1/2}$ Ag-atom photoexcitation to the $^2P_{1/2,1/2}$, $^2P_{3/2,3/2}$, $^2P_{3/2,1/2}$ excited states [45b]; (ii) exciplex formation involving at least two exciplex electronic states and involving one or more rare gas atoms for each excited Ag atom, possibly followed by vibrational relaxation of the excited exciplex states (a minimum of two excited exciplex states is strongly suggested by the emission spectra and lifetime measurements [45c]); (iii) exciplex fluorescence, again involving at least two excited exciplex electronic states, to the ground (repulsive) state; (iv) dissociation of the repulsive ground exciplex state resulting in Ag-atom mobilization.
Further to point (ii) of Scheme A, exciplex formation between matrix-entrapped metal atoms and rare gas matrix atoms has been suggested to explain certain effects observed in the absorption and luminescence spectra of matrix-isolated metal atoms [45a,c,d].

45 (a) D.M. Kolb and D. Leutleff, Chem. Phys. Lett., 55 (1978) 264; (b) F. Forstmann, D.M. Kolb, D. Leutloff and W. Schulze, J. Chem. Phys., 66 (1977) 2806; (c) G.A. Ozin, G. Kenney-Wallace, T. Huber, J. Farrell and S. Mitchell, to be published; (d) A.A. Belyaeva, Y.B. Predtechenskii and L.D. Shcherba, Opt. Spectrosc., 34 (1973) 21.